Supplementary file accompanying "**Rapid solid-state sintering in volcanic systems**" by Amy

G. Ryan[1], James K. Russell[1] and Michael J. Heap[2]

[1]Volcanology and Petrology Laboratory, EOAS, University of British Columbia, 2020-2207

Main Mall, Vancouver, BC, V6T 1Z4, Canada

[2]Institut de Physique de Globe de Strasbourg (UMR 7516 CNRS, Université de

Strasbourg/EOST), 5 rue René Descartes, 67084 Strasbourg, France

*Corresponding author: aryan@eoas.ubc.ca

This file contains:

Supplement 1. Physical properties of Mount St. Helens (MSH) cataclasites [Table S1] and

additional scanning electron microscopy (SEM) images of sintered MSH rocks [Figure

S1]

Supplement 2. Grain size distribution [Figure S2] and mineralogy of hot isostatic pressing (HIP)

experimental materials [Table S2]

Supplement 3. Extended methodology and model development [Figure S3]

Supplement 4. Additional scanning electron microscopy (SEM) images of sintered HIP materials

[Figure S4]

Supplement 1. Physical properties and SEM images of Mount St. Helens (MSH) cataclasites.

**Supplementary Table S1.** Physical properties of Mount St. Helens samples.

Sample	Bulk Density (ρ_b, kg/m^3) [a]	Total Porosity [b]	Permeability (m^2)[c]
7_5j_4	2605	0.032	1.26×10^{-16}
7_5j_1	2603	0.033	2.00×10^{-16}
7_4b_3	2521	0.064	6.31×10^{-16}
7_3c_4	2397	0.121	2.00×10^{-15}
7_3c_1	2227	0.183	2.51×10^{-14}
5_2b(2)_1	1983	0.264	6.31×10^{-14}
4_3a(2)_2	1896	0.282	6.31×10^{-14}
4_3a(2)_1	1791	0.321	1.26×10^{-12}

Notes: Full dataset in Ryan et al. (2018). Values are representative of MSH materials.

[a] $\rho_b = m / (\pi r^2 l)$ using the mass (m), radius (r) and length (l) of the sample core.

[b] Isolated porosities are <0.02.

[c] Steady-state measurement (see Supplement 3).
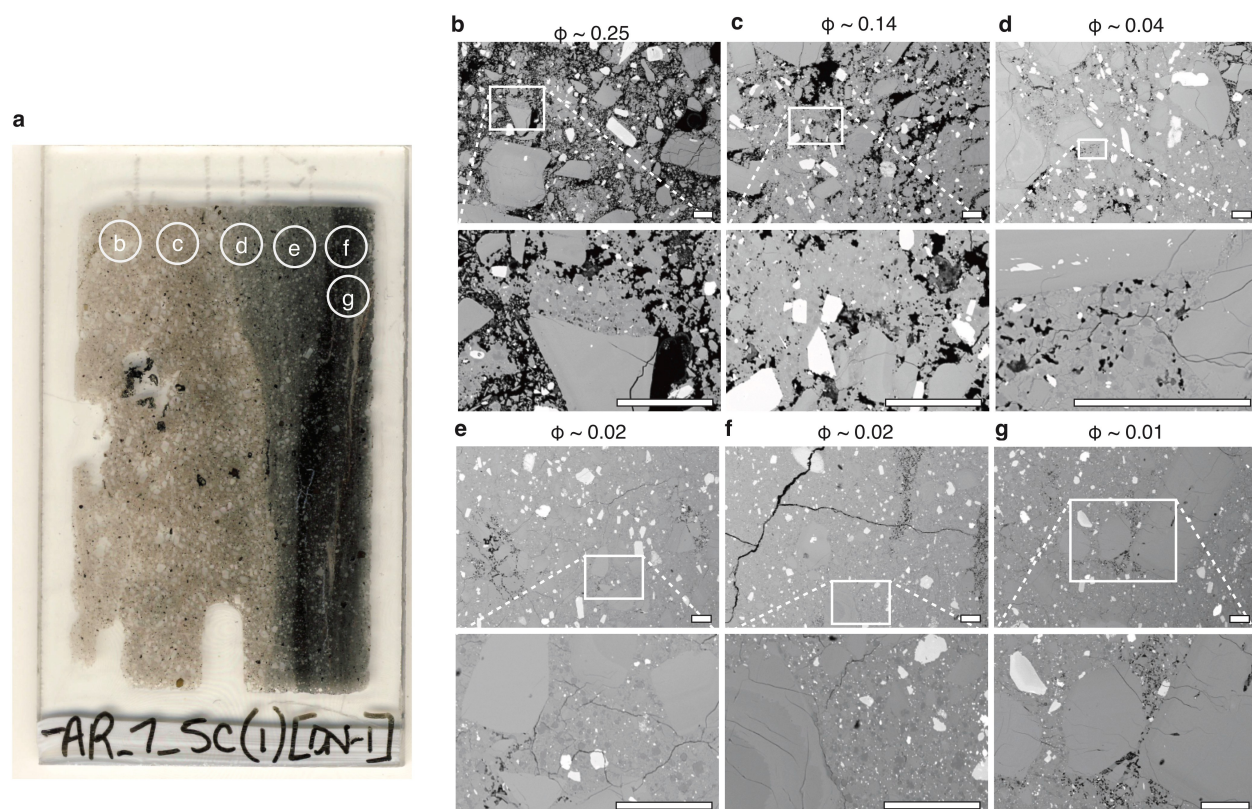
Figure S1: SEM transect of lithified MSH sample. (a) Photomicrograph of a thin section that grades from poorly consolidated to lithified gouge. The thin section and SEM images are oriented parallel to the extrusion direction. Labeled circles are locations of SEM image pairs **(b-g)**. Top image of each pair shows the lithified crystalline material at lower magnification image. White boxes show the location of higher magnification images (bottom image of pairs). Total - porosity values (ϕ) (measured by image analysis) are given. From **(b)** to **(g)** the proportion of sintered material increases, and the porosity decreases. In the most sintered materials **(e-g)**, small irregular voids in the consolidated matrix and small fractures are the only void spaces. Scale bars are 100 μm.

Supplement 2. Grain size distribution and mineralogy of HIP experimental materials.
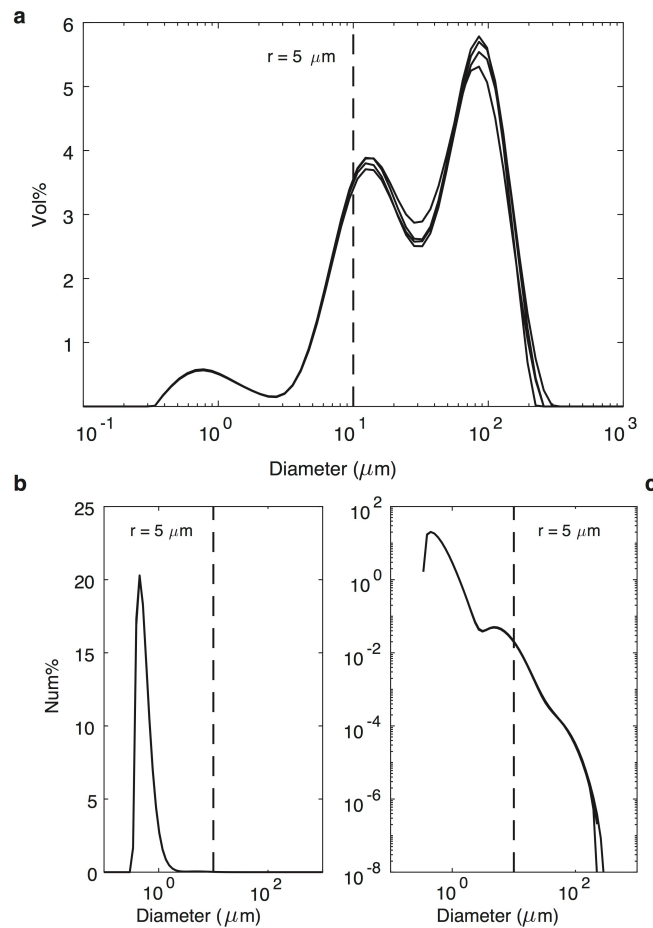
Figure S2: Particle size distribution curves for HIP experimental material. MSH dacitic fault gouge sieved to <125 μm. Particle size distributions for 5 aliquots were measured using a laser particle size analyzer. Dashed lines show where particle radius is 5 μm. **(a)** Volume percent (vol%) of particles of a given diameter in the starting material. Data from different aliquots agree well (curves overlap). The greatest volume contribution is from particles >30 μm in diameter. **(b)** The same data shown as number percent (assuming spherical particles; num%) on both linear (left) and log (right) axes. Most particles in the sieved gouge have diameters <10 μm.

Table S2: Mineralogy of HIP starting material and experimental products.

Supplementary Table S2. Mineralogy of HIP starting material and experimental products.

Mineral	Starting Material (wt%)	HIP 1 (wt%)	HIP 1 [a] (wt%)	HIP 4 (wt%)
Plagioclase (An$_{30-50}$)	45.2	41.7	41.3	43.9
Potassic feldspar (~Or$_{32}$)	14.8	17.5	19.3	17.1
SiO$_2$ polymorphs	21.2	19.0	21.9	22.4
FeMg silicates	16.1	17.7	13.8	15.4
FeTi oxides	2.8	4.1	3.7	1.3
Total	100.1	100.0	100.0	100.0

Note: Mineral constituents determined by Rietveld refinement of X-Ray Diffraction (XRD) spectra (Raudsepp et al., 1999).

[a] Repeat analysis.

Supplement 3. Extended methodology and model development.

Physical Property Measurements

The top and bottom surfaces of the cylindrical HIP canisters were removed and 3-4 cores (1-2 cm length, 1 cm diameter) were drilled from the experimental products. One core from each HIP sample was used for thin sectioning and subsequent SEM imaging (e.g., Fig. 1).

The ends of two cores from each HIP sample were ground to parallel surfaces, and the mass, length and diameter of the cores were measured using a high-precision balance and digital calipers. These data were used to calculate the bulk volume and bulk density (ρ_b) of each core (Table 1). The propagated uncertainty in bulk density measurements is 20-70 kg/m^3. The skeletal volumes of cores were measured using a Micromeritics AccuPyc II 1340 helium pycnometer at the University of British Columbia (Canada). The uncertainty in these measurements is 0.02-0.04 cm^3. The volume of a known mass of the starting material was also measured by helium pycnometry to retrieve the powder density (ρ_p= 2716 kg/m^3; uncertainty is <10 kg/m^3). The connected, total and isolated porosities of the cores was calculated using the measured bulk, skeletal and powder (true) densities (Table 1). The propagated uncertainty for porosities is <0.01.

Permeabilities were measured using a benchtop gas (nitrogen) permeameter at the Institut de Physique du Globe de Strasbourg (IPGS) at the Université de Strasbourg (France). All permeabilities were measured on dry samples (dried in a vacuum oven at 40°C for at least 48 h) at room temperature and a confining pressure of 1 MPa. Prior to their measurement, the samples were kept under a confining pressure of 1 MPa for 1 h to ensure microstructural equilibration. Following microstructural equilibration, measurements of permeability were performed using the steady-state flow method. Steady-state volumetric flow rate measurements were taken (using a flowmeter) under several pore pressure gradients. These data allow us to calculate permeability

whilst checking whether the data require auxiliary corrections, such as the Klinkenberg and Forchheimer corrections. In all cases, the Forchheimer correction was required and the true permeability is taken as the inverse of the y-intercept of the best-fit linear regression in the plot of $1/k_{gas\_raw}$ as a function of the volumetric flow rate, where k_{gas_raw} is the uncorrected (raw) gas permeability determined for each of the pore pressure gradients implemented during the experiment.

Model Development

We use the experimental conditions and the final density of the experimental products to develop a model for densification by solid-state sintering. An empirical equation, termed the "semilogarithmic law" (e.g., Coble, 1961; Vieira and Brook, 1984; Rahaman 2003) is commonly used to fit experimental hot (isostatic) pressing data and has the form:

$$\rho_r = \rho_0 + \alpha \ln\left(\frac{t}{t_0}\right) \qquad \text{Eq. (S1) and Eq. (1)}$$

where ρ_0 is the relative density at an initial time t_0, ρ_r is relative density at time t, and α is a fit parameter dependent on the experimental temperature and pressure (e.g., Rahaman, 2003). We include T and P in α by using established thermodynamic and kinetic relationships, including those in general forms of the power law creep equations (e.g. Rybacki and Dresen, 2004):

$$\frac{d\rho(T)}{dt}\frac{d\rho}{dt} \approx a \exp\left(\frac{b}{T}\right) \qquad \text{Eq. (S2a)}$$

$$\frac{d\rho(P)}{dt}\frac{d\rho}{dt} \approx P^c \qquad \text{Eq. (S2b)}$$

$$\frac{d\rho}{dt} = \frac{K}{t} = a \exp\left(\frac{b}{T}\right) P^c \frac{1}{t} \qquad \text{Eq. (S2c)}$$

Integration yields:

$$\rho_r = a \exp\left(\frac{b}{T}\right) P^c \ln(t) + \ln\left(\frac{t}{t_0}\right) + d \qquad\qquad \text{Eq. (S3)}$$

and at $t = 1$ the value of $\rho_r = \rho_i / \rho_p$ (the initial relative density where ρ_i is the initial density and ρ_p is the powder density (Table 1)). Then for $t \geq 1$ the Eq. S3 becomes:

$$\rho_r = \frac{\rho_i}{\rho_p} + a \ \exp\left(\frac{b}{T}\right) P^c \ln(t) \qquad\qquad \text{Eq. (S4) and Eq. (2)}$$

The model, which is dependent on temperature (T; K), pressure (P; MPa), and time (t; s), has 3 unknown parameters (a, b, c). Solving for the unknown parameters we find $a = 0.039 \pm 0.019$, $b = -3064 \pm 290$ and $c = 0.482 \pm 0.064$. The model fits our experimental data to within uncertainty (Fig. 3).

Model Limitations

Experimental data has been shown to deviate from Eq. 1 where $\rho_r > 0.95$ (e.g. Vieira and Brook, 1984). The deviation is attributed to the isolation of small pore spaces (Coble, 1961). We therefore Eq. 2 is not applicable at $\rho_r > 0.97$, where $\rho_r = 0.97$ ($\phi = 0.03$) is the percolation threshold where pores become isolated (Wadsworth et al., 2016, 2017). Additionally, the limited range of our experimental P-T conditions means that when applied far from these conditions, Eq. 2 may be poorly unconstrained.
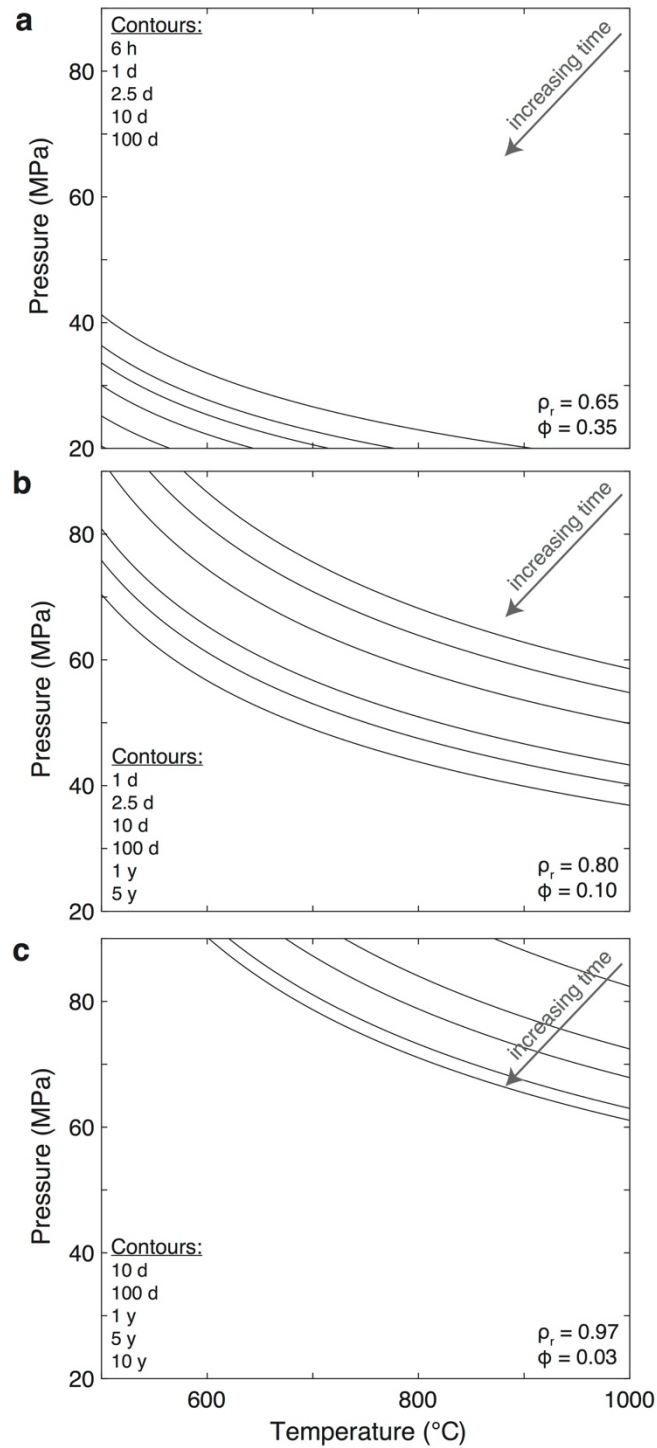
Ryan et al. (American Mineralogist): Figure S3

Figure S3: Temperature (T) – pressure (P) sintering maps. Contours show the time to reach a relative density of **(a)** 0.65, **(b)** 0.80 and **(c)** 0.97. At low T-P conditions sintering time is not controlled by P (steep slope of contours), but a 100 °C increase in T is sufficient to reduce sintering time. Above ~750 °C, the effect of T on sintering time diminishes (contours flatten). Increasing P reduces sintering time at these conditions.

Supplement 4. Additional SEM images of HIP materials.
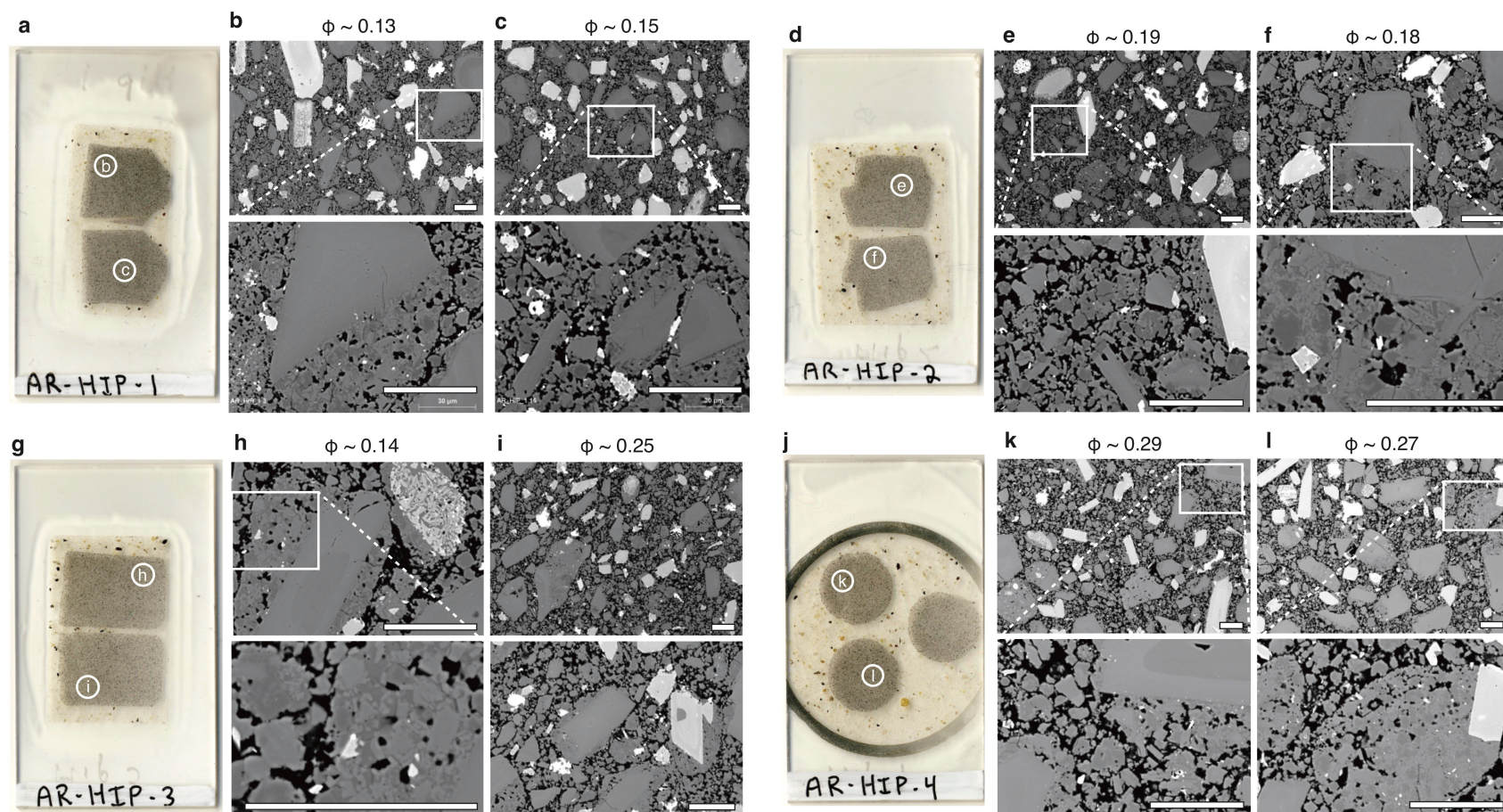
Figure S4: Additional SEM images of HIP products. (a,d,g,j) Photomicrographs of thin sections of HIP products (labeled). Figure layout as in Fig. S1. The material subjected to the greatest experimental conditions (HIP1; Table 1) shows the greatest proportion of sintered material and the least pore space. The opposite is true for the sample sintered at the least extreme experimental conditions (HIP4; Table 1). Because the applied pressure was isotropic there is no preferred orientation of crystals or pore spaces. Scale bars are 50 μm.